Tamper indicating gold nanocup plasmonic films

Brent M. DeVetter, Bruce E. Bernacki, Wendy D. Bennett, Alan Schemer-Kohrn, and Kyle J. Alvine[a)]
Pacific Northwest National Laboratory, Richland, Washington 99354, USA

(Received 2 November 2016; accepted 24 January 2017; published online 13 February 2017)

The spectral signatures of nanoplasmonic films are both robust and tailorable with optical responses ranging from the visible to the near-infrared. We present the development of flexible, elastomeric nanoplasmonic films consisting of periodic arrays of gold nanocups as tamper indicating films. Gold nanocups have polarization-sensitive optical properties that may be manufactured into films that offer unique advantages for tamper indication. These flexible films can be made quickly and at low-cost using the commercially available monodisperse polystyrene nanospheres through self-assembly followed by plasma etching, metal deposition, and lift-off from a sacrificial substrate. The polarization- and angle-dependent optical spectroscopic measurements were performed to characterize the fabricated films. Using polarization-sensitive hyperspectral imaging, we demonstrate how these films can be applied to tamper indication and counterfeit resistance applications. *Published by AIP Publishing*. [http://dx.doi.org/10.1063/1.4975936]

Plasmonic nanomaterials have shown a great deal of promise in applications ranging from robust color displays,[1] colorimetric sensors,[2] and highly sensitive chemical detection.[3] When illuminated with certain frequencies of light, the free electron gas in subdiffraction-limited metallic nanostructures coherently and collectively oscillates.[4] This effect, called the localized surface plasmon resonance (LSPR), grants the ensembles of coinage metal nanostructures unique macroscopic optical properties that may be engineered for exciting photonics applications. In this paper, we focus on the design, fabrication, and characterization of anisotropic plasmonic nanostructures—gold nanocups—applied to tamper indication and counterfeit resistant proof-of-concept applications.

Advances in tamper indication technologies are highly sought after in areas as varied as nuclear nonproliferation,[5] supply chain management and logistics,[6] food and pharmaceutical safety,[7] and consumer anti-identity theft protection.[8] To help combat illicit activities in these areas, the plasmonic nanomaterials offer exciting possibilities. Nano-based tamper indicating films are particularly attractive because it is exceedingly difficult to counterfeit nanostructured films without advanced instrumentation and highly specialized knowledge. In the case of plasmonic nanofilms, the unique spectral response is dependent on factors such as the sample orientation, the shape and size of the plasmonic metal, and the refractive index of the backing film material. To date, researchers have investigated tamper indicating substrates using the precisely patterned plasmonic nanoparticles primarily based on the near-field coupling between structures.[9] This approach can provide anti-tampering properties but is limited in terms of practical application because it is prohibitively expensive to fabricate substrates consisting of single particles positioned at nanometer resolution. In contrast, our focus here is on the manufacturability and demonstration of low-cost nanoplasmonic films with tamper indicating far-field optical properties.

The optical properties of half-shell, or nanocup, plasmonic nanostructures were pioneered by Halas and coworkers.[10,11] Gold nanocups are akin to 3D split ring resonators—which are essentially the optical equivalent to LC circuit oscillators—popularized and heavily studied by the metamaterials and microwave engineering communities.[12] We have previously demonstrated the LC oscillator equivalence of L-shaped gold patterned films fabricated using nanoimprint lithography.[13] The asymmetrical nature of gold nanocups results in two distinct plasmon modes. Two degenerate magnetic dipole modes occur when the electron gas oscillates along the curvature of the gold surface, whereas the electric dipole mode occurs when the electron gas oscillates across the gap of the nanocup's rim.[10] As we will discuss, the electric dipole mode is highly polarization-sensitive for gold nanocup films, whereas the magnetic dipole mode is polarization-insensitive. The presence of modes that are orthogonally sensitive to polarized radiation allows us to harness their spectral properties for tamper sensing applications in which a sample has been damaged by way of peeling, tearing, or cutting and subsequently repaired or reseated to conceal the damage.

The basis for the initial nanoplasmonic gold nanocup studies by Halas and coworkers focused on two primary routes of fabrication. The first approach involved drying randomly dispersed polystyrene nanospheres on a substrate followed by metal sputtering.[11] The resulting substrate consisted of a gold film with randomly patterned gold nanocup features. The nanocups were then transferred from the substrate to a transparent, flexible substrate by pouring polydimethylsiloxane (PDMS) onto the substrate, allowing it to cure, and carefully lifting off the nanocups from the substrate. The second method utilized core-shell gold-silica nanoshells synthesized in wet chemistry. The core-shell nanoshells were randomly dispersed on a substrate followed with an argon reactive ion etch, thereby removing half of the

[a)]Author to whom correspondence should be addressed. Electronic mail: kyle.alvine@pnnl.gov

gold shell, while the silica-core remained intact.[10] Other wet chemical synthesis techniques to fabricate colloidal nanocups have been since developed, showing a great deal of flexibility in the design and fabrication of these structures.[14]

The tamper indicating nanoplasmonic films discussed here were fabricated (Figure 1) using colloidal lithography rather than random dispersion.[11,15] This technique works via the self-assembly of monodisperse polymeric nanospheres into a hexagonally close-packed (hcp) monolayer configuration. The self-assembled nanospheres were isotropically plasma etched to form a periodic array of nanosized non-touching polystyrene spheres. Magnetron sputter coating of a thin layer of gold is followed at varying angles to tune the optical anisotropy. Colloidal lithography offers excellent uniformity across macroscopic films, as compared to random dispersion and is significantly less expensive than top-down approaches such as electron beam lithography.[16] As a proof-of-concept, the fabricated films used gold as the plasmonically active metal to facilitate the polarization-dependent optical properties. Gold is an excellent starting material to work with because it exhibits tunable resonances from the visible to near-infrared and is resistant to oxidation. Nonetheless, from a manufacturing perspective, gold is less attractive due to its relatively high cost. As this technology gets closer to the production stage, alternative plasmonic materials are desirable to reduce manufacturing costs. Aluminum, in particular, has recently shown great promise as a plasmonic metal[17] and can be similarly patterned into films using colloidal lithography followed by metal sputtering. While the optical properties of aluminum are distinct from that of gold, we suggest it as a potential route forward. Furthermore, colloidal lithography techniques are translatable to large-scale manufacturing processes such as roll-to-roll processing,[18] in which large-area nanostructured films could be produced using the self-assembled nanosphere templating.

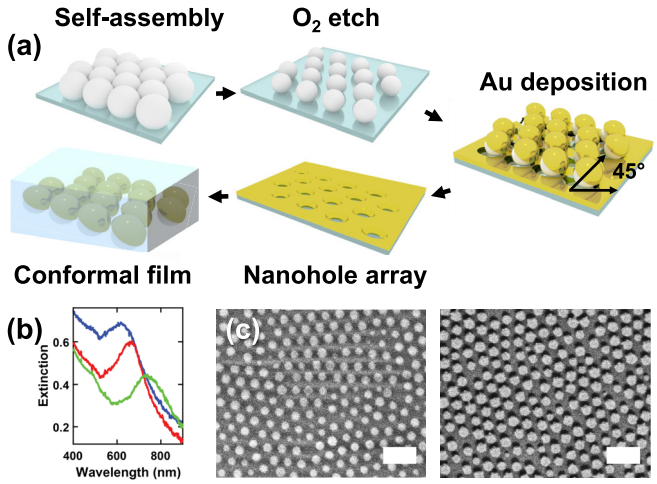

FIG. 1. (a) Schematic of nanoplasmonic film fabrication. Polystyrene nanospheres were self-assembled onto a sacrificial glass wafer via spin-coating followed by an oxygen plasma etch. The resulting nanopatterned substrate consisting of equally spaced nanospheres was then coated with a thin layer of gold (15–20 nm) at 45°. After metal deposition, PDMS was poured onto the patterned substrate, allowed to cure, and then peeled off, resulting in a patterned nanohole array (on glass) and an elastomeric conformal film of nanocups. (b) Extinction spectra of representative nanoplasmonic substrates on glass (before lift-off) with plasmon resonances at 620 nm (blue), 670 nm (red), and 740 nm (green). (c) Representative scanning electron micrograph of the etched polystyrene-coated substrate (left) and the substrate after metal deposition (right). Scale bar: 250 nm.

The fabrication steps for manufacturing gold nanocup arrays are outlined in Figure 1. Briefly, commercially purchased (Bangs Laboratories, Inc.) monodisperse polystyrene nanospheres (99 nm diameter) were spun-cast onto a plasma-cleaned 2-in. glass wafer to form an hcp monolayer of nanospheres. The resulting monolayer was heated (2 min, 107 °C) in an oven just above the glass transition temperature of polystyrene to improve adhesion to the glass surface. Size-reduction of the nanospheres was performed via an oxygen plasma (Diener Zepto) for 300–400 s with a chamber pressure of ~0.2 mbar. Finally, a 15–20 nm layer of gold was deposited at an angle of 45° using magnetron sputtering. We found the adhesion of gold to polystyrene to be sufficient, such that an adhesion metal layer (such as Cr) was unnecessary. The extinction spectra of representative samples with plasmon resonances at 620 nm, 670 nm, and 740 nm are shown in Figure 1(b). To further validate the formation of nanocup structures, scanning electron microscopy was performed before and after metallization (Figure 1(c)).

The metallized glass substrate acts as a sacrificial rigid, transparent substrate that must be removed for tamper indication studies. An elastomeric nanoplasmonic film was made by pouring PDMS (Sylgard 182) directly onto the surface of the metallized substrate and allowing it to cure (40 °C for >12 h). The resulting nanoplasmonic film is flexible and relatively transparent (~90% transmission from 400 to 800 nm). Here, the transmission spectra of the flexible film were measured at normal incidence. The LSPR of the flexible film was 570 nm, and the residual nanohole array left after lift-off was measured to be 540 nm (Figure 2(a)). Although not demonstrated here, the nanohole array on glass could be further used for various optical/chemical sensing applications and is a less expensive alternative to substrates fabricated using the focused ion beam milling.

The polarization-dependent optical properties of the nanoplasmonic film were studied by illuminating the sample with light from a halogen lamp and coupling that light into a multimodal fiber bundle. After passing the light through a linear polarizer in free-space, the light was collimated (~3.5 mm diameter at the sample) and normally incident upon the film. The film was mounted such that the projection of the metal deposition direction was 90° with respect to the

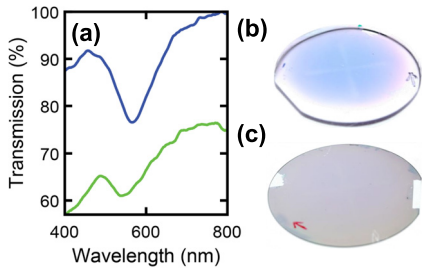

FIG. 2. (a) Transmission spectra (normal incidence, unpolarized light) of a representative nanoplasmonic film (blue, $\lambda_{LSPR} = 570$ nm) and the spectra of the remaining plasmonic nanohole substrate (on glass) after lift-off (green, $\lambda_{LSPR} = 540$ nm). Photographs of (c) a nanoplasmonic PDMS film and (d) a metallized glass substrate after lift-off. Arrows in the photographs indicate the direction in which the sample was tilted at 45° during metallization.

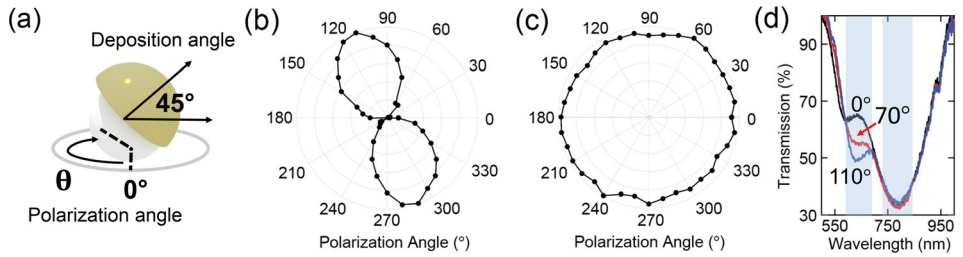

FIG. 3. (a) Schematic of the nanoplasmonic film indicating the polarization angle (θ) for normally incident, linearly polarized light. The measured normalized intensity of the (b) electric dipole mode (630 nm) and (c) magnetic dipole mode (785 nm) as a function of polarization angle. (d) Transmission spectra of the nanoplasmonic film with polarization angles 0° (black), 70° (red), and 110° (blue), illustrating the polarization-dependent optical properties for each mode.

origin of the polarizer. The polarization angle was then varied from 0° to 360° in a left-handed sense (Figure 3(a)). The transmitted light was collected into a multimodal fiber connected to a spectrometer. The intensity of the excited dipole modes was quantified by integrating the electric and magnetic spectral bands for each polarization. In Figures 3(b) and 3(c), the intensities of the integrated bands were plotted as a function of polarization angle θ. As described by Halas and coworkers,[10] the magnetic dipole modes (785 nm) are degenerate, lower-energy modes, as compared to the single higher-energy electric dipole mode (630 nm). The magnetic dipole mode is unique to asymmetric nanostructures and offers polarization-independent spectral properties. In contrast, the electric dipole mode shows a characteristic dipolar $\cos^2\theta$ scattering pattern tilted from its axis of symmetry as a function of gold deposition angle.[10] The scattering pattern (Figure 3(b)) illustrates how the absence of the excited electric dipole mode can be used to create silent spectral regions such as from $0° < \theta < 60°$ as well as non-silent regions such as from $70° < \theta < 150°$, where the electric dipole mode is most strongly excited. In contrast, the magnetic dipole mode is excited regardless of the polarization of incident light. The study by Halas[10] provides additional insight into factors such as roughness and the effects of substrates on the far- and near-field properties of nanocups. To further illustrate the two distinct modes, the transmission spectra for three different polarization angles are shown in Figure 3(d).

The angle-dependent spectral properties of these films with a fixed linear polarization (90°) were also investigated. The sample was mounted on a rotatable stage and allowed to rotate from slightly more than −25° to 25° in 0.5° increments. Optical extinction was calculated from the measured transmission spectra using Beer's law and plotted as a 2D spectral map of sample angle versus wavelength. Extinction was used rather than transmission to assist with visualizing the influence of the plasmon modes as a function of angle. We observe that the excitation of the modes is not symmetrical about 0°, possibly due to experimental variation in the quality of the metal deposition across the film or inaccuracies in our alignment of the deposition angle with respect to our optical setup. The transmission spectra (Figure 4(b)) were acquired in the same manner as the polarization-dependent measurements. At higher angles such as 65°, thin-film interference effects due to the metallized polystyrene nanospheres were also observed. Given the parameters of metal deposition angle, sample angle, and polarization angle, it is possible to maximize or minimize the contribution of the electric dipole mode. For tamper indication, it is desirable to orient the sample such that the polarization-dependent electric dipole mode is maximized.

Tamper indication studies were performed by collecting light passed through a linear polarizer to a hyperspectral imaging setup.[19] Here, a commercial hyperspectral camera (Headwall Photonics, Inc.) was used to collect data cubes consisting of position x, position y, and spectral data, as described previously.[20] The samples were illuminated at 45° and the camera was mounted above the sample so as to collect scattered light. Two orthogonally (horizontal and vertical) polarized hyperspectral images were acquired and

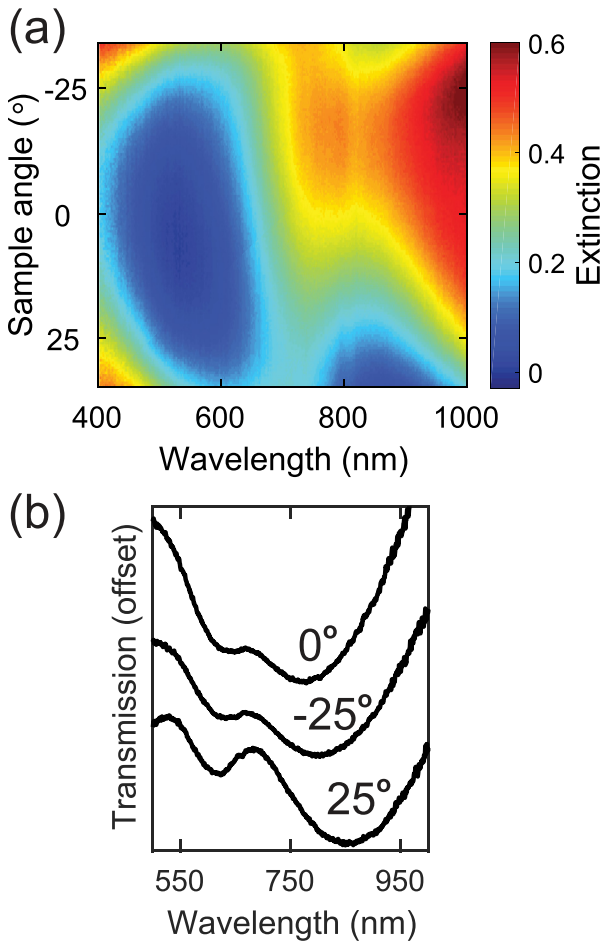

FIG. 4. (a) Experimentally measured 2D map of optical extinction for sample angle versus wavelength with a representative PDMS-transferred nanoplasmonic film. The metal deposition angle of the nanocups was aligned with the linear polarizer at 90°. (b) Transmission spectra (offset for clarity) of film for three sample angles.

subtracted from each other. The principal component analysis (PCA) was performed on the resulting hyperspectral cube, and the first three principal components were color-mapped to red (R), green (G), and blue (B) to form a tamper indicating image. PCA is a chemometric technique that reorients data to a new orthogonal axis such that variance across data is maximized.[21] This allows us to visualize tampering with minute spectral changes in portions of the hyperspectral image. In the first case (Figure 5(a)), a single circular cutout was taken from the nanoplasmonic film and rotated 180° from the orientation of the surrounding film, so as to flip the orientation of the gold nanocups within that region. The entire film was then repaired by immersing it in additional PDMS and allowing it to cure. While it is possible to visually see that a cut has been made onto the film, it is nearly impossible to visually discern that the orientation of the nanocups has been reversed. Furthermore, with improved cutting and tampering processes, it would be straightforward to completely conceal outline of the cutout and hide all visual evidence of tampering. By processing two polarized hyperspectral images and applying PCA (Figure 5(b)), however, it is possible to clearly see the evidence of tampering.

The next tampering studies involved four cutouts removed and oriented in different positions to further illustrate our ability to detect tampering (Figures 5(c) and 5(d)). In contrast to the single cutout sample, these samples were not repaired with PDMS and were only reseated in new positions to illustrate the additional contribution of scattering at the interface. In Figure 5(c), the two cutouts colorized in green were essentially reseated in their original position, having the same polarization signature, whereas the two cutouts in blue were rotated approximately 90°, resulting in a strongly evident spectral difference in polarization. The highly scattering interface at the perimeter of the cut also adds additional contrast to the image further providing the evidence of tampering. In Figure 5(d), the cutouts were rotated gradually from approximately 0° to 90°. In this case, the first principal component was discarded and the following three principal components were mapped to R, G, and B. This shows that it is possible to detect tampering even in cases where efforts were made to patch or repair the damage.

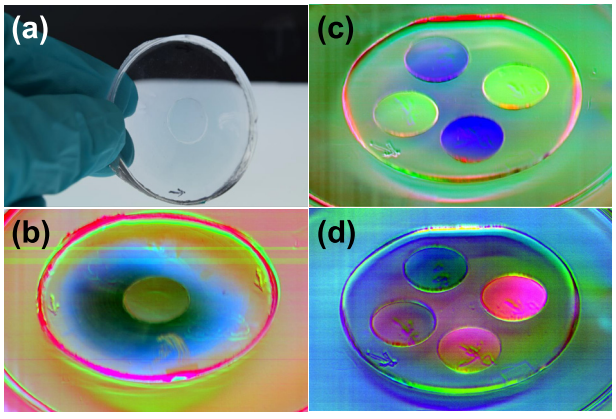

FIG. 5. (a) Photograph of tampered nanoplasmonic film with an arrow indicating the direction of metal deposition for the non-cutout region. (b) Color-mapped PCA image with R, G, and B corresponding to the first three principal components of the differenced polarization images acquired with a hyperspectral camera. The center cutout was rotated 180° and repaired with PDMS. While the outline of the cutout is visible, it is nearly impossible upon visual inspection to determine that the nanocups have been rotated without performing PCA analysis. Two example configurations of cutouts (c) orthogonal and (d) gradual degrees of rotation to the reseated cutouts.

In conclusion, we have demonstrated the fabrication of elastomeric nanoplasmonic films using scalable colloidal lithography as a robust polarization-sensitive tamper indicating film. These films can be fabricated with a wide variety of resonances ranging from the visible to the near-infrared. Unique spectral signatures are also possible by way of fabricating multi-resonant nanoplasmonic films, making it even more difficult counterfeit these films. Furthermore, the polarization-dependent optical properties are tunable through parameters such as metal deposition angle and sample orientation. We demonstrated using a hyperspectral camera and post processing of two orthogonal polarization data cubes that it is possible to detect both abrupt and gradual alterations to these films. With further manufacturing effort, it would be possible to produce large area seals, tags, and other tamper indicating and counterfeit resistant products that could be applied to a wide variety of applications.

This research was performed at the Pacific Northwest National Laboratory (PNNL), which is operated by the Battelle Memorial Institute for the Department of Energy (DOE) under Contract No. DE-AC05-76RL01830. The authors gratefully acknowledge support from the PNNL National Security Directorate Laboratory Directed Research and Development (LDRD) funding.

[1]L. Duempelmann, D. Casari, A. Luu-Dinh, B. Gallinet, and L. Novotny, ACS Nano **9**(12), 12383 (2015).
[2]N. S. King, L. Liu, X. Yang, B. Cerjan, H. O. Everitt, P. Nordlander, and N. J. Halas, ACS Nano **9**(11), 10628 (2015); T.-W. Chang, X. Wang, A. Hsiao, Z. Xu, G. Lin, M. R. Gartia, X. Liu, and G. L. Liu, Adv. Opt. Mater. **3**(10), 1397 (2015).
[3]J.-F. Li, J. R. Anema, T. Wandlowski, and Z.-Q. Tian, Chem. Soc. Rev. **44**(23), 8399 (2015).
[4]S. A. Maier, *Plasmonics: Fundamentals and Applications* (Springer, 2007).
[5]K. J. Alvine, J. D. Suter, B. E. Bernacki, and W. D. Bennett, Proc. SPIE **9456**, 94560C (2015).
[6]J. Stradley and D. Karraker, IEEE Trans. Compon. Packag. Technol. **29**(3), 703 (2006).
[7]C. Shillingford, C. W. Russell, I. B. Burgess, and J. Aizenberg, ACS Appl. Mater. Interfaces **8**(7), 4314 (2016).
[8]B. Reardon, K. Nance, and S. McCombie, paper presented at the 2012 45th Hawaii International Conference on System Sciences, 2012.
[9]N. Makoto, T. Naoya, and O. Motoichi, J. Opt. **14**(9), 094002 (2012).
[10]N. S. King, Y. Li, C. Ayala-Orozco, T. Brannan, P. Nordlander, and N. J. Halas, ACS Nano **5**(9), 7254 (2011).
[11]N. A. Mirin and N. J. Halas, Nano Lett. **9**(3), 1255 (2009).
[12]S. Han, L. Cong, H. Lin, B. Xiao, H. Yang, and R. Singh, Sci. Rep. **6**, 20801 (2016).
[13]K. J. Alvine, B. E. Bernacki, W. D. Bennett, D. J. Edwards, A. Mendoza, and J. D. Suter, Appl. Phys. Lett. **102**(20), 201115 (2013).
[14]A. Ihsan, H. Katsiev, N. Alyami, D. H. Anjum, W. S. Khan, and I. Hussain, J. Colloid Interface Sci. **446**, 59 (2015).
[15]B. Ai, H. Möhwald, D. Wang, and G. Zhang, Adv. Mater. Interfaces **4**, 1600271 (2017); L. Wang, R. J. H. Ng, S. S. Dinachali, M. Jalali, Y. Yu, and J. K. W. Yang, ACS Photonics **3**(4), 627–633 (2016).
[16]F. Yue, D. Wen, J. Xin, B. D. Gerardot, J. Li, and X. Chen, ACS Photonics **3**(9), 1558 (2016).

[17]L. Zhou, Y. Tan, J. Wang, W. Xu, Y. Yuan, W. Cai, S. Zhu, and J. Zhu, Nat. Photonics **10**(6), 393 (2016); M. W. Knight, N. S. King, L. Liu, H. O. Everitt, P. Nordlander, and N. J. Halas, ACS Nano **8**(1), 834 (2014).
[18]Y. Guo, S. Batra, Y. Chen, E. Wang, and M. Cakmak, ACS Appl. Mater. Interfaces **8**(28), 18471 (2016).
[19]J. A. Richards and X. Jia, *Remote Sensing Digital Image Analysis: An Introduction*, 4th ed. (Springer-Verlag, Berlin, 2006).
[20]B. E. Bernacki, N. C. Anheier, A. Mendoza, B. G. Fritz, and T. J. Johnson, Proc. SPIE **8018**, 80180K (2011).
[21]R. G. Brereton, *Applied Chemometrics for Scientists* (Wiley, 2007).